INTERNATIONAL JOURNAL FOR NUMERICAL METHODS IN FLUIDS
Int. J. Numer. Meth. Fluids 2005; **47**:1043–1051
Published online in Wiley InterScience (www.interscience.wiley.com). DOI: 10.1002/fld.925

On MILES based on flux-limiting algorithms‡

F. F. Grinstein[1,*,†], C. Fureby[2] and C. R. DeVore[1]

[1] *LCP&FD, U.S. Naval Research Laboratory, Washington, DC 20375-5344, U.S.A.*
[2] *Weapons and Protection, The Swedish Defence Research Agency, FOI, SE-172 90, Stockholm, Sweden*

SUMMARY

Non-classical large eddy simulation (LES) approaches based on using the unfiltered flow equations instead of the filtered ones have been the subject of considerable interest during the last decade. In the monotonically integrated LES (MILES) approach, flux-limiting schemes are used to emulate the characteristic turbulent flow features in the high-wave number end of the inertial subrange region. Mathematical and physical aspects of *implicit* sub grid scale modelling using nonlinear flux-limiters are conveniently addressed using the modified LES-equation formalism. In this study, the performance of MILES is demonstrated as a function of the flux-limiting scheme in selected representative case studies. Published in 2005 by John Wiley & Sons, Ltd.

KEY WORDS: MILES; flux-limiting; implicit LES; monotonic; turbulence

BACKGROUND

High Reynolds (*Re*) number turbulent flows are of considerable importance in many fields of engineering, geophysics, and astrophysics. Capturing the dynamics of all relevant scales based on the numerical solution of the Navier–Stokes (NS) equations constitutes direct numerical simulation (DNS), which is prohibitively expensive for practical flows at moderate-to-high *Re*. Large eddy simulation (LES) is an effective intermediate approach between DNS and Reynolds-averaged Navier–Stokes modelling, capable of simulating flow features which cannot be handled with RANS such as flow unsteadiness and strong vortex–acoustic couplings. Desirable modelling choices involve selecting an appropriate discretization of the flow problem at hand, such that the LES cut-off lies within the inertial subrange, and ensuring that a smooth transition can be enforced at the cut-off. The main assumptions of LES are that: (i) transport

*Correspondence to: F. F. Grinstein, LCP&FD, U.S. Naval Research Laboratory, 4555 Overlook Avenue SW, Washington, DC 20375-5344, U.S.A.
†E-mail: grinstein@lcp.nrl.navy.mil

Contract/grant sponsor: Los Alamos National Laboratory
Contract/grant sponsor: Naval Research Laboratory

Received 27 April 2004
Revised 10 December 2004
Accepted 13 December 2004

Published in 2005 by John Wiley & Sons, Ltd.

is largely governed by large-scale unsteady features and that such dominant features of the flow can be resolved, and (ii) the less-demanding accounting of the small-scale flow features can be undertaken by using suitable sub-grid scale (SGS) models. In the absence of an accepted universal theory of turbulence, the development and improvement of SGS models are unavoidably pragmatic and based on the rational use of empirical information. Classical approaches have included many proposals ranging from inherently limited eddy-viscosity formulations to more sophisticated and accurate mixed models, see e.g. Reference [1] for a recent survey. The main drawback of mixed models relates to their computational complexity, and ultimately, to the fact that well-resolved (discretization-independent) LES is prohibitively expensive for the practical flows of interest at moderate-to-high *Re*.

Recognizing the aforementioned difficulties but also motivated by new ideas pioneered by Boris and collaborators [2], several researchers have abandoned the classical LES formulations and started employing the unfiltered flow equations instead of the filtered ones. Major focus of the new approaches [3] has been on the inviscid inertial-range dynamics and regularization of the under-resolved flow, based on *ab initio* scale separation with additional assumptions for stabilization, or applying monotonicity via nonlinear limiters that implicitly act as a filtering mechanism for the small scales—the original proposal of Boris *et al.* [2]. The latter concept goes back to the 1950s to von Neumann and Richtmyer [4], who used artificial dissipation to stabilize finite-difference simulations of flows involving shocks. This artificial dissipation concept also motivated Smagorinsky [5] in developing his scalar viscosity concept based up on the principles of similarity in the inertial range of 3D isotropic turbulence.

In what follows, we use the modified equation formalism to carry out a formal comparative analysis of conventional LES and MILES. The performance of MILES is examined for selected representative case studies to demonstrate MILES dependence on the flux-limiting specifics. We conclude by pointing out some outstanding open issues of the implicit LES (ILES) concept.

CONVENTIONAL LES

For simplicity, we restrict the discussion to incompressible flows described by the NS momentum balance equation, $\partial_t(\mathbf{v}) + \nabla\cdot(\mathbf{v}\otimes\mathbf{v}) = -\nabla p + \nabla\cdot\mathbf{S}$, in conjunction with the incompressibility (or divergence) constraint $\nabla\cdot\mathbf{v} = 0$, where $\otimes$ denotes the tensorial product, and $\mathbf{S} = 2\nu\mathbf{D}$ and $\mathbf{D} = \frac{1}{2}(\nabla\mathbf{v} + \nabla\mathbf{v}^{\mathrm{T}})$ are the viscous-stress and strain-rate tensors. The conventional LES procedure [1] involves three basic ingredients: (i) low-pass filtering, (ii) finite volume, element or difference discretization, and (iii) *explicit* SGS modelling to close the low-pass filtered equations. Applying (i) and (ii) to the NS equations—using a second-order accurate finite volume algorithm, and rewriting the results in terms of the *modified equations* (ME), i.e. the equations satisfied by the numerical solutions being actually calculated, yields [6, 7]

$$\partial_t(\bar{\mathbf{v}}) + \nabla\cdot(\bar{\mathbf{v}}\otimes\bar{\mathbf{v}}) = -\nabla\bar{p} + \nabla\cdot\bar{\mathbf{S}} - \nabla\cdot\mathbf{B} + \mathbf{m}^{\nu} + \boldsymbol{\tau}$$

where $\mathbf{B} = \overline{\mathbf{v}\otimes\mathbf{v}} - \bar{\mathbf{v}}\otimes\bar{\mathbf{v}}$, $\mathbf{m}^{\nu} = [G*, \nabla](\mathbf{v}\otimes\mathbf{v} + p\mathbf{I} - \mathbf{S})$, $\boldsymbol{\tau} = \nabla\cdot[[\frac{1}{6}\nu\nabla^3\mathbf{v} - \frac{1}{8}\nabla^2\mathbf{v}](\mathbf{d}\otimes\mathbf{d}) + \cdots]$ are the SGS stress tensor, commutation error term, and the total (convective and viscous) truncation error, respectively. Here, $\mathbf{I}$ is the unit tensor and $\mathbf{d}$ is the topological vector connecting neighbouring control volumes, and, $[G*, \nabla]f = \overline{\nabla f} - \nabla\bar{f}$. The commutation error term is often

lumped together with the SGS force $\nabla\cdot\mathbf{B}$, prior to modelling, and hence a generalized SGS stress tensor $\mathbf{B}$ needs to be prescribed in terms of discretized filtered fields for closure of the new equations—which constitutes (iii) above.

IMPLICIT LES

A key self-consistency issue required in the conventional LES approach involves separating the computing effects of its three basic elements: filtering, discretization, and reconstruction. Filtering and reconstruction contributions must be resolved, i.e. their effective contributions in the ME above must be larger than the total truncation error $\boldsymbol{\tau}$. Also, the interactions of their upper range of represented (but inaccurate) scales must be addressed—in addition to those between resolved and SGSs. However, we could argue that discretization could implicitly provide $\mathbf{B}$ if nonlinear stabilization can be achieved algorithmically via a particular class of numerical algorithms or based on regularizing the discretization of the conservation laws. In fact, the ME suggest that most schemes can potentially provide built-in or implicit SGS models enforced by the discretization errors $\boldsymbol{\tau}$ provided that their leading order terms are dissipative. We are thus led to the natural question: to what extent can we avoid the (explicit) filtering and modelling phases of LES and focus on the implicit $\mathbf{B}$ provided by a suitably chosen discretization scheme?

Not all implicitly implemented SGS models are expected to work: the numerical scheme has to be constructed such that the leading order truncation errors satisfy physically required SGS properties, and hence nonlinear discretization procedures will be required here. The analogy to be recalled is that of shock-capturing schemes designed under the requirements of convergence to weak solution while satisfying the entropy condition [8]. Non-oscillatory finite-volume (NFV) algorithms can be viewed as relevant for ILES of turbulent flows based on *nonlinear* implicit SGS modelling [7, 9], if we focus on two distinct inherent *physical* SGS features to be emulated:

- the anisotropy of high-*Re* turbulent flows in the high-wave number end of the inertial subrange region, characterized by very thin filaments of intense vorticity and largely irrelevant internal structure, embedded in a background of weak vorticity, e.g. Reference [10],
- the discrete nature of laboratory observables (finite fluid portions transported over finite periods of time are always measured).

We thus require that ILES be based on NFV numerics having a *sharp velocity-gradient capturing capability* operating at the smallest resolved scales. By focusing on the inviscid inertial-range dynamics and on adaptive regularization of the under-resolved flow, ILES thus follows very naturally on the historical precedent of using these kinds of schemes for shock capturing—in the sense that requiring emulation (near the cut-off) of the high wave number end features of the inertial subrange region of turbulent flows is analogous to spreading the shock width to the point that it can be resolved by the grid.

An intriguing MILES feature is the convection discretization that implicitly generates a nonlinear tensor-valued eddy-viscosity, which acts predominantly to stabilize the flow and suppress unphysical oscillations. The ME analysis of MILES [7] draws on the fact that FV methods filter the NSE over non-overlapping computational cells Ω_P with the typical

dimension $|\mathbf{d}|$. In the finite-volume context, discretized equations are obtained from the NS equations using Gauss' theorem and by integrating over time with a multistep method. To close the discretization equations, interface fluxes need to be reconstructed from the dependent variable values at adjacent cells. The methods available for constructing implicit SGS models by means of the leading order truncation errors are generally restricted to nonlinear high-resolution methods for the convective fluxes (at least second-order accurate on smooth solutions while giving well-resolved, non-oscillatory discontinuities) [8]. In addition, these schemes are required to provide a leading order truncation error that vanishes as $\mathbf{d} \to \mathbf{0}$ so that it remains consistent with the NS equations and with conventional LES models. We focus here on certain flux-limiting and correcting methods.

To this end, we introduce a flux-limiter Γ that combines a high-order convective flux-function $\mathbf{v}_f^H$ that is well-behaved in smooth flow regions, with a low-order dispersion-free flux-function $\mathbf{v}_f^L$, being well-behaved near sharp gradients, so that the flux-function becomes $\mathbf{v}_f = \mathbf{v}_f^H - (1-\Gamma)[\mathbf{v}_f^H - \mathbf{v}_f^L]$. Choosing the particular flux-limiting scheme also involves specific selections for $\mathbf{v}_f^L$ and $\mathbf{v}_f^H$. In our ME analysis involving second-order fluxes [7], $\mathbf{v}_f^H$ and $\mathbf{v}_f^L$ have been assumed to be based on linear interpolation and upwind-biased piecewise constant approximation, respectively. Comparing the resulting ME [7] with the corresponding analysis of the momentum equation in the framework of the conventional LES approach suggests that the MILES ME incorporate additional dissipative and dispersive terms, and we can consistently identify the leading order convective truncation error terms, as providing the implicit SGS stress terms $\mathbf{B} = \mathbf{C}(\nabla\mathbf{v})^T + (\nabla\mathbf{v})\mathbf{C}^T + \chi^2(\nabla\mathbf{v})\,\mathbf{d}\otimes(\nabla\mathbf{v})\,\mathbf{d}$, where $\mathbf{C} = \chi(\mathbf{v}\otimes\mathbf{d})$ is a generalized eddy viscosity and $\chi = \frac{1}{2}(1-\Gamma)(\beta^- - \beta^+)$, with $\beta^\pm = \frac{1}{2}(\mathbf{v}_f\,d\mathbf{A} \pm |\mathbf{v}_f\,d\mathbf{A}|)/|\mathbf{v}_f\,d\mathbf{A}|$.

The implicit SGS stress tensor $\mathbf{B}$ can be decomposed into $\mathbf{B}^{(1)} = \mathbf{C}(\nabla\mathbf{v})^T + (\nabla\mathbf{v})\mathbf{C}^T$ and $\mathbf{B}^{(2)} = \chi^2(\nabla\mathbf{v})\,\mathbf{d}\otimes(\nabla\mathbf{v})\,\mathbf{d}$, in which the former is a tensor-valued eddy-viscosity model, while the latter is of a form similar to a structural type (e.g. scale similarity) model [1]. The inherently dissipative nature of this implicit SGS model has been demonstrated in Reference [6] based on analysis of its associated effective viscosity. Detailed properties of the implicit SGS model are related to the flux-limiter Γ and to the choice of low- and high-order schemes; they also relate as well to other specific features of the scheme—e.g. monotonicity, l_1-contraction, local monotonicity preservation, and gridding. We have illustrated above and discussed elsewhere [6, 7], how some of these properties can directly affect the implicit SGS modelling effectiveness in the MILES context. MILES performance as a function of flux limiter is discussed below.

MILES BASED ON ONE-DIMENSIONAL FLUX-LIMITING

Here we address effects of variations in the use of one-dimensional (1D) flux-limiter Γ. We first consider high-resolution schemes that can be formulated using the ratio of consecutive gradients, $r = \delta\mathbf{v}^n_{P-1/2}/\delta\mathbf{v}^n_{P+1/2} = (\mathbf{v}^n_P - \mathbf{v}^n_{P-1})/(\mathbf{v}^n_{P+1} - \mathbf{v}^n_P)$. Examples of flux-limiters that fit into this category are (1) the minmod limiter $\Gamma = \max(0, \min(1, r))$ [11], (2) the superbee limiter, $\Gamma = \max(0, \max(\min(2r, 1), \min(r, 2)))$ [11], (3) the van-Leer limiter, $\Gamma = (r + |r|)/(1 + |r|)$ [11], (4) the van-Albada limiter, $\Gamma = (r + r^2)/(1 + r^2)$ [12], and (5) the GAMMA limiter $\Gamma = (1-k)/kr[\theta(r) - \theta(r - (k/(1-k)))] + \theta(r - (k/(1-k)))$ [13], where k is a parameter of the scheme such that $k \in [0, 1]$, and θ is the Heavyside function. Note that when $k = 0.5$, this scheme becomes total variational diminishing (TVD).

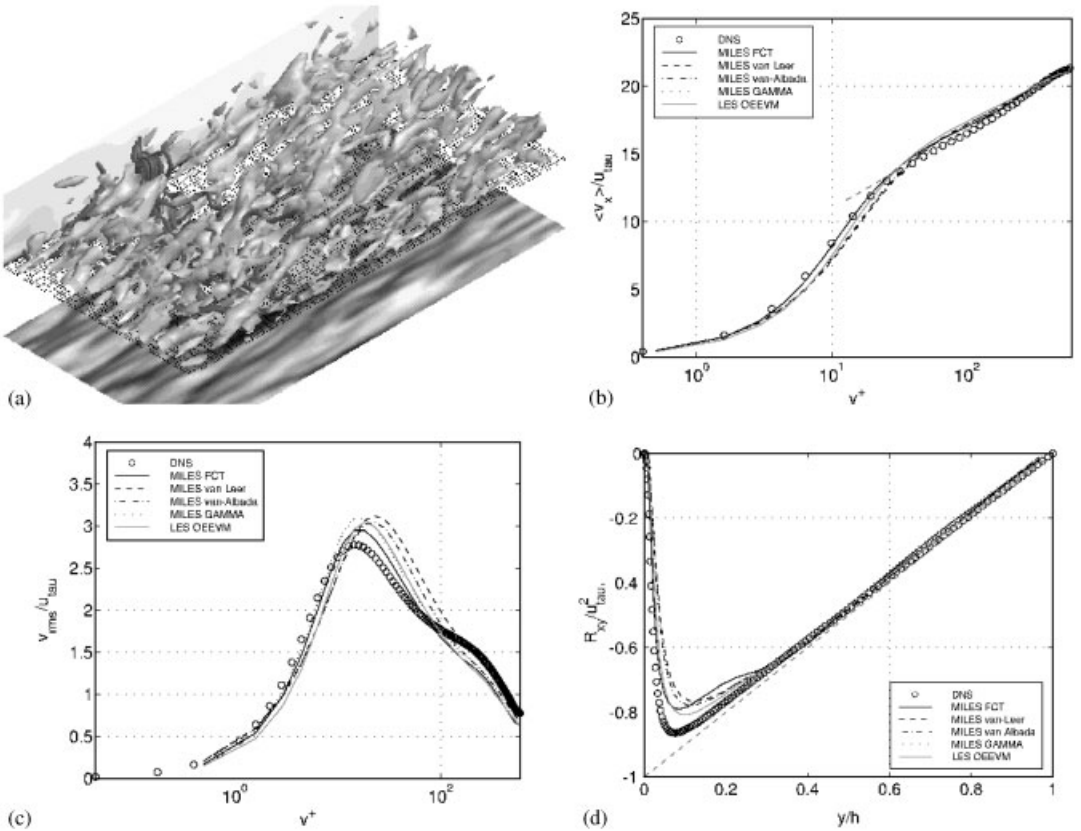

Figure 1. MILES of $Re_t = 590$ channel flow; dependence on choice of flux-limiter at the 60^3 grid; $y^+ = v/u_\tau$ is the wall normal co-ordinate.

Some of these limiters can be effectively compared in terms of Sweby diagrams [14], plotting the TVD constraint $\mathrm{TV}(\mathbf{v}^{n+1}) \leqslant \mathrm{TV}(\mathbf{v}^n)$, where $\mathrm{TV}(\mathbf{v}^n) = \sum_P \|\mathbf{v}^n_{P+1} - \mathbf{v}^n_P\|$, reformulated as $0 \leqslant |\Gamma(r), \Gamma(r)/r| \leqslant 2$ [11]. From this perspective, the effective diffusivity of the schemes decreases as the flux-limiters approach that of the superbee limiter, which results in the least diffusive scheme. We can also consider other schemes, such as flux corrected transport (FCT) [15], and piecewise parabolic method (PPM) [16], which can also use a similar flux-limiting-type formalism based on $\mathbf{v}_\mathrm{f} = \mathbf{v}^\mathrm{H}_\mathrm{f} - (1-\Gamma)[\mathbf{v}^\mathrm{H}_\mathrm{f} - \mathbf{v}^\mathrm{L}_\mathrm{f}]$, but for which the flux limiter cannot simply be formulated in terms of the ratio of consecutive gradients, r. The latter schemes are locally monotonicity-preserving, i.e. given the solution $\mathbf{v}^{n+1}_P = H(\mathbf{v}^n_{P-k}, \mathbf{v}^n_{P-k+1}, \ldots, \mathbf{v}^n_{P+k})$, if $\mathbf{v}^0_P \geqslant \mathbf{v}^0_{P+1}$, then $\mathbf{v}^n_P \geqslant \mathbf{v}^n_{P+1}$ for all P and n. Being less diffusive, schemes based on local constraints are to be preferred for MILES.

The global performance of MILES as a function of flux-limiter is documented in Figure 1, showing studies of fully developed turbulent channel flow at a friction-velocity based Re of $Re_t = 590$, compared with DNS results [17]. The channel has a length of $6h$ and a width of $3h$ and is confined between two parallel plates $2h$ apart, where h is the channel half-width. The flow is driven by a fixed mass flow in the streamwise ($\mathbf{e}_x$) direction. The friction velocity is

$u_\tau = \sqrt{\tau_w}$, where τ_w is the wall-shear stress. We vary the mass flow to obtain the target friction-velocity-based Re. Other specifics of the channel flow calculations are discussed in detail elsewhere (e.g. Reference [7]); the simulations were carried out on 60^3 and 48^3 grids. The grid consists of uniform spacing in the streamwise and spanwise directions, whereas geometrical progression in the $\mathbf{e}_y$-direction is used to appropriately cluster the grid near the walls to resolve the velocity gradients with uniform spacing in the streamwise and spanwise directions. Periodic boundary conditions are employed in both streamwise and spanwise directions, together with no-slip conditions in the wall-normal directions. In all calculations, a wall-model [18] is used to emulate the near-wall features that cannot be resolved on the grid.

Figure 1(a) shows the main flow features of the channel flow in terms of vortex lines, contours of $v_x - \langle v_x \rangle$ on the side and contours of v at the bottom, and isosurfaces of the second invariant of the velocity gradient $Q = 1/2(\|\mathbf{W}\|^2 - \|\mathbf{D}\|^2)$. Q shows, together with the v-contours, that the flow is dominated by wall-shear-induced vortical structures. Figures 1(b)–(d) show the time-averaged streamwise velocity $\langle v_x \rangle$ (integrated over x and z), the resolvable axial rms-velocity fluctuation $v_x'^+ = v_x'/u_\tau$, where $v_x' = \sqrt{\langle (v_x - \langle v_x \rangle)^2 \rangle}$, and the resolvable shear stress $R_{xy} = \langle v_x' v_y' \rangle$, respectively, for different implicit sub-grid models based on the FCT, van-Leer, van-Albada and GAMMA limiters, respectively. The agreement between MILES, DNS data, and conventional LES results (using the one equation eddy viscosity model, OEEVM) is generally good, with the most apparent deviations found in the resolved axial rms-velocity fluctuation. Moreover, the log-law, $\langle v_x \rangle^+ = \kappa^{-1} \ln(y^+) + B$, is generally well-predicted with $B \approx 5.2 \pm 0.1$ and $\kappa \approx 0.41 \pm 0.01$. The influence of the flux limiter is comparatively small but has been observed to be sensitive to the wall-normal resolution (cf. References [7, 18]). From Figure 1 it is evident that the van-Leer limiter is too diffusive, producing poor velocity profiles, while both FCT and GAMMA produce velocity profiles that agree well with the reference DNS data.

MILES BASED ON MULTI-DIMENSIONAL FLUX-LIMITING

FCT was originally developed to accurately solve the conservation equations of Eulerian fluid dynamics without violating the positivity of mass and energy, particularly in the vicinity of shock waves and other discontinuities [15]. The goal of the flux-correction procedure is to provide as accurate a solution to the original equation as is consistent with maintaining positivity and local monotonicity everywhere. For certain multi-dimensional applications, this limiter and its underlying integration scheme can be employed in a serial fashion to each of the co-ordinate directions in turn, using operator splitting. Other problems, however, call for a fully multi-dimensional approach. These include both incompressible or nearly incompressible flows, and flows with a high degree of symmetry. Zalesak [19] analysed Boris and Book's 1D FCT limiter [15], identified the tests inherent in it, and showed why a reformulation was needed to extend the FCT approach to multi-dimensional situations. He provided such a formulation, showed that his new limiter could be made equivalent to the original, and then illustrated it with several one- and two-dimensional examples. Usage of this FCT limiter has shown that it preserves positivity but not monotonicity, yielding solutions with numerical ripples of significant amplitude in many cases; an effective modification of Zalesak's limiter, which contributes greatly towards preserving monotone profiles, was introduced through the addition of a prelimiting step based on the original 1D limiter, thus ensuring that both positivity (when required) and monotonicity of the solutions are locally preserved [20].

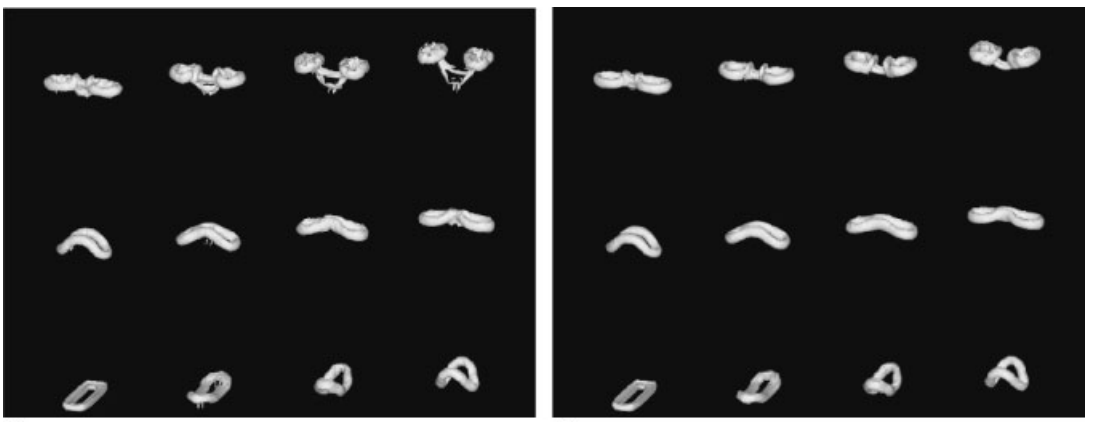

Figure 2. Self-deformation, reconnection, and subsequent bifurcation of an isolated vortex ring are shown. The ring is puffed from a Mach 0.6 air jet whose aspect ratio is 4:1. Isosurfaces of the vorticity magnitude are shown at 15% of the peak initial vorticity. Time increases from left to right and from bottom to top in the figure: (a) used Zalesak's flux limiter, which preserves positivity but not monotonicity; and (b) used the monotone flux limiter, which involves a prelimiting step using (monotonicity preserving) 1D FCT in each cross-stream direction.

Figure 2 illustrates the effectiveness of these multi-dimensional limiters in the context of MILES of a subsonic rectangular jet [21, 22]. An initially laminar air jet at standard temperature and pressure issues from a rectangular nozzle of aspect ratio 4:1 at Mach 0.6. The quiescent background gas also is at STP. In order to focus on the dynamics of the individual vortex rings of the jet, an isolated ring is puffed out by closing off the inflow boundary after a finite time equal to the ratio of the jet equivalent diameter to the flow speed. The evolution of the ring is then followed as it convects downstream. The key underlying aspects of the vortex ring bifurcation process were first demonstrated with MILES [21], including self-induced deformation, reconnection, bridging and threading—mechanisms which could not be captured by the laboratory visualizations.

The numerical studies used 2D FCT in the cross-stream planes and a 1D FCT [15] for the streamwise direction. A $150 \times 110 \times 110$ grid was used to represent the domain, with the cells evenly spaced in the shear-flow region of the jet and geometrically stretched in the cross-stream directions outside. The Courant number was 0.5. Fixed mass density and velocity conditions were specified on the boundary cells defining the jet orifice, with free-slip conditions enforced elsewhere on the entrance plane. Convective conditions were imposed on those quantities at the outflow boundary, and all variables satisfy stagnation-flow conditions at the cross-stream boundaries. The pressure satisfies the inviscid 1D pressure equation at the jet orifice and a non-reflecting condition at the outflow boundary.

Time sequences of isosurfaces of the vorticity magnitude are shown in Figure 2, obtained using Zalesak's limiter and the monotone limiter in the 2D FCT module. In the figures, time increases from left to right and from bottom to top. The bottom-most six frames in each figure show the self-induced deformation and axis switching of the vortex ring. The highly curved corners accelerate ahead of the ring sides and towards the centreline, pulling the minor axis sides along with them. This process bends the ring along its major axis. The increasing

curvature at the midpoints of the major sides accelerates those portions streamwise towards the leading minor sides but away from the jet centreline. This results in a nearly planar, axis-switched configuration of the vortex ring at frame 6. This early evolution is essentially identical in the two cases, save for some intermittent, small-scale, numerical features evident with Zalesak's limiter.

Subsequently, the ring's new major sides pinch together and reconnect, forming a pair of vortex rings linked on the underside by two thin threads. This is shown in the following (top) four panels of Figure 2. While both simulations clearly show the bifurcation of the ring, the fine structure associated with the threads bridging the two daughter rings increasingly differs between the two limiters. Zalesak's limiter permits fluctuations on the threads of vorticity, which show up as spikes attached to the isosurfaces and lead at frame 12 to the fragmenting of the threads, and (as suggested in Figure 2(a)) the two daughter vortex rings irrevocably separate at later times. In contrast, with the monotone 2D limiter the fine structure is cleanly and clearly represented through frame 12, the vorticity threads remain intact, and the daughter rings stay in close proximity to one another, leading to significantly different later vortex dynamics [21]. This example dramatically demonstrates that the dynamical behaviour of the system, above and beyond the aesthetics of the simulation results, can be influenced significantly by the implicit SGS model associated with the flux limiter specifics. Studies testing various different flux-limiting approaches in the context of canonical benchmark problems are reported separately [23].

OUTLOOK

MILES seeks to emulate the flow features in the high-wave number end of the inertial subrange of turbulent flows—characterized by thin filaments of intense vorticity embedded in a background of weak vorticity. We have proposed that emulation of the latter feature be the requirement for the more general concept of nonlinear implicit SGS modelling in the context of finite-volume formulations. In the more general ILES approach thus defined, the functional reconstruction of the convective flux functions is carried out via high-resolution nonlinear FV schemes incorporating a sharp velocity-gradient capturing capability operating at the smallest resolved scales. By focusing on the inviscid inertial-range dynamics and on regularization of the under-resolved flow, ILES follows up very naturally on the historical precedent of using this kind of numerical schemes for shock-capturing.

In MILES, the effects of SGS physics on the resolved scales are incorporated in the functional reconstruction of the convective fluxes using locally-monotonic methods. Analysis based on the modified equations shows that MILES, based on a particular class of flux-limiting schemes, provides an implicitly implemented anisotropic SGS model dependent on the specifics of the particular numerical scheme—i.e. on the flux-limiter Γ, on the choice of low- and high-order schemes, and on the gridding. Selected representative case studies were used here to demonstrate the dependence of the MILES performance on flux-limiting specifics, suggesting the important role of local monotonicity preservation, and indicating that local (vs non-local TVD) constraints are to be preferred.

ACKNOWLEDGEMENTS

This work was completed while one of us (FFG) was Orson Anderson Distinguished Visiting Scholar at IGPP, Los Alamos National Laboratory, on Sabbatical leave from the U.S. Naval Research Laboratory.

Support from the Los Alamos National Laboratory base research program and from the Office of Naval Research through the Naval Research Laboratory 6.1 Computational Physics task area is also greatly appreciated.

REFERENCES

1. Sagaut P. *Large Eddy Simulation for Incompressible Flows*. Springer: New York, 2002.
2. Boris JP, Grinstein FF, Oran ES, Kolbe RJ. New insights into large eddy simulations. *Fluid Dynamics Research* 1992; **10**:199.
3. Grinstein FF, Karniadakis GEm (eds). Alternative LES and hybrid RANS/LES. *Journal of Fluids Engineering* 2002; **124**:821.
4. von Neumann J, Richtmyer RD. A method for the numerical calculation of hydrodynamic shocks. *Journal of Applied Physics* 1950; **21**:232.
5. Smagorinsky J. The beginnings of numerical weather prediction and general circulation modelling: early recollections. *Advances in Geophysics* 1983; **25**:3.
6. Fureby C, Grinstein FF. Monotonically integrated large eddy simulation of free shear flows. *AIAA Journal* 1999; **37**:544.
7. Fureby C, Grinstein FF. Large eddy simulation of high Reynolds number free and wall bounded flows. *Journal of Computational Physics* 2002; **181**:68.
8. Godunov SK. Reminiscences about difference schemes. *Journal of Computational Physics* 1999; **153**:6–25.
9. Margolin LG, Rider WJ. A rationale for implicit turbulence modelling. *International Journal for Numerical Methods in Fluids* 2002; **39**:821.
10. Jimenez J, Wray A, Saffman P, Rogallo R. The structure of intense vorticity in isotropic turbulence. *Journal of Fluid Mechanics* 1993; **255**:65.
11. Hirsch C. *Numerical Computation of Internal and External Flows*. Wiley: New York, 1999.
12. Albada GD, van Leer B, Roberts WW. A comparative study of computational methods in cosmic gas dynamics. *Astronomy and Astrophysics* 1982; **108**:76.
13. Jasak H, Weller HG, Gosman AD. High resolution NVD differencing scheme for arbitrarily unstructured meshes. *International Journal for Numerical Methods in Fluids* 1999; **31**:431.
14. Sweby PK. High resolution schemes using flux limiters for hyperbolic conservation laws. *SIAM Journal on Numerical Analysis* 1984; **21**:995.
15. Boris JP, Book DL. Flux corrected transport I, SHASTA, a fluid transport algorithm that works. *Journal of Computational Physics* 1973; **11**:38.
16. Colella P, Woodward P. The piecewise parabolic method (PPM) for gas dynamic simulations. *Journal of Computational Physics* 1984; **54**:174.
17. Moser RD, Kim J, Mansour NN. Direct numerical simulation of turbulent channel flow up to $Re_t = 590$. *Physics of Fluids* 1999; **11**:943.
18. Fureby C, Alin N, Wikström N, Menon S, Persson L, Svanstedt N. On large eddy simulations of high *Re*-number wall bounded flows. *AIAA Journal* 2004; **42**:457.
19. Zalesak ST. Fully multidimensional flux-corrected transport algorithms for fluids. *Journal of Computational Physics* 1979; **31**:335.
20. DeVore CR. An improved limiter for multidimensional flux-corrected transport. *NRL Memorandum Report NRL/MR/6440-98-8330*, Washington, DC, 1998.
21. Grinstein FF. Self-induced vortex ring dynamics in subsonic rectangular jets. *Physics of Fluids* 1995; **7**:2519.
22. Grinstein FF. Vortex dynamics and entrainment in regular free jets. *Journal of Fluid Mechanics* 2001; **437**:69.
23. Grinstein FF, Margolin L, Rider W (eds). *Implicit Large Eddy Simulation*: *Capturing the Turbulent Flow Dynamics, Chapter 4a*. Cambridge University Press: Cambridge, 2005, in press.